

Taming a Retrieval Framework to Read Images in Humanlike Manner for Augmenting Generation of MLLMs

Suyang Xi

Merwinn520@outlook.com
Emory University
Atlanta, USA

Yiqing Ni

The Hong Kong Polytechnic University
Hong Kong, China

Chenxi Yang

University of Electronic Science and Technology of China
Chengdu, China

Hong Ding

University of Illinois Chicago
Chicago, USA

Catherine C. Liu

The Hong Kong Polytechnic University
Hong Kong, China

Yunhao Liu

The Hong Kong Polytechnic University
Hong Kong, China

Chengqi Zhang

The Hong Kong Polytechnic University
Hong Kong, China

Abstract

Multimodal large language models (MLLMs) often fail in fine-grained visual question answering, producing hallucinations about object identities, positions, and relations because textual queries are not explicitly anchored to visual referents. Retrieval-augmented generation (RAG) alleviates some errors, but it fails to align with human-like processing at both the retrieval and augmentation levels. Specifically, it focuses only on global-level image information but lacks local detail and limits reasoning about fine-grained interactions. To overcome this limitation, we present *Human-Like Retrieval-Augmented Generation (HuLiRAG)*, a framework that stages multimodal reasoning as a “what–where–reweight” cascade. Queries are first anchored to candidate referents via open-vocabulary detection (*what*), then spatially resolved with SAM-derived masks to recover fine-grained precision (*where*), and adaptively prioritized through the trade-off between local and global alignment (*reweight*). Mask-guided fine-tuning further injects spatial evidence into the generation process, transforming grounding from a passive bias into an explicit constraint on answer formulation. Extensive experiments demonstrate that this human-like cascade improves grounding fidelity and factual consistency while reducing hallucinations, advancing multimodal question answering toward trustworthy reasoning.

CCS Concepts

- Computing methodologies → Artificial intelligence; • Information systems → Information retrieval.

Keywords

Multimodal retrieval-augmented generation, Explainable recommendation, Visual grounding

1 Introduction

Recent advancements in multimodal LLMs (MLLMs) such as GPT-4o, Gemini, Claude 3, and LLaVA have shown impressive capabilities in a variety of tasks [5, 6, 19, 42, 49, 50]. However, these models

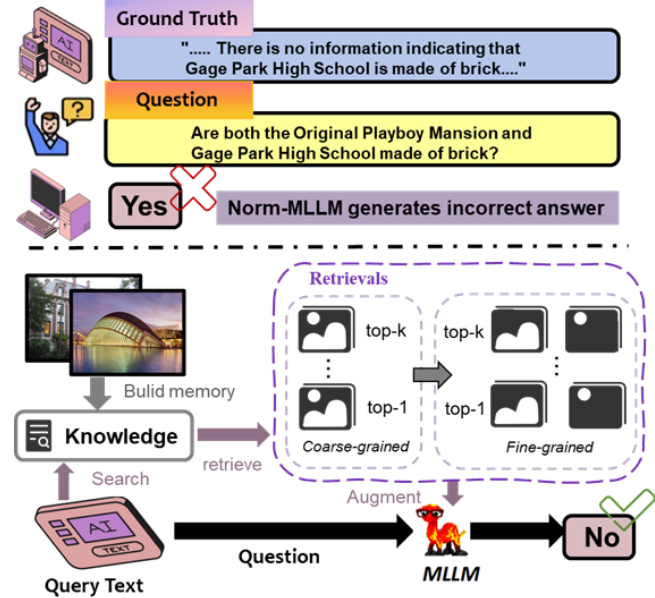


Figure 1: Standard MLLMs struggle with factual VQA due to inadequate perceptual grounding. Our method equips LLMs with the ability to ‘read’ images by dynamically retrieving and aligning semantically relevant visual regions, enabling evidence-based reasoning.

continue to struggle with fine-grained, fact-based Visual Question Answering (VQA), particularly in scenarios requiring precise, region-specific visual understanding [38, 39, 47]. A key limitation of current systems is their inability to dynamically process and validate visual information, relying instead on pre-trained, static knowledge representations [12, 33, 53]. This results in two primary challenges: (1) *hallucinations*, where models generate information not grounded in the input data [52, 54, 73], and (2) *rigid reasoning*, characterized by the lack of flexible, real-time integration of visual

input and contextual information, akin to human working memory processes [13, 25, 58]. Although current multimodal models have made considerable progress in many areas [9, 41, 67], these perceptual and reasoning gaps remain a fundamental obstacle in fine-grained VQA tasks.

To address static knowledge limitations in multimodal reasoning, Retrieval-Augmented Generation (RAG) systems augment Multimodal Large Language Models (MLLMs) by dynamically retrieving external evidence[64]. Current approaches can be divided into three paradigms: (1) *Efficient Search*: Optimized via Maximum Inner Product Search (MIPS)[21] or graph-based ANNs[69] for low-latency retrieval; (2) *Modality Specialization*: Leveraging domain-specific embeddings (e.g., CLIP[51], BLIP[37]) for cross-modal alignment; (3) *Adaptive Re-ranking*: Refining results via precision filters[68]. However, current retrieval-augmented generation (RAG) systems predominantly operate at the image-level granularity, which proves inadequate for complex multimodal tasks demanding fine-grained understanding [1]. Although some works have begun exploring more flexible retrieval approaches, for example, KURAG [71] advances retrieval flexibility through knowledge unit fusion (joint embeddings of text snippets and entity-linked images) [15], it still fails to achieve true sub-image-level retrieval (e.g., localized regions or instance-specific patches) [48]. This limitation starkly contrasts with human visual cognition, which dynamically integrates multi-granular information, seamlessly shifting between global scenes, local details, and instance features based on contextual demands [34].

Fundamentally, existing RAG frameworks exhibit a cognitive-system divergence in compositional reasoning mechanisms. Humans consciously manipulate mental imagery [34] to compositionally explore cross-modal content across granularities, whereas existing RAG approaches tend to entangle signals from multiple modalities into a unified representation space [74], simplifying the problem to facilitate subsequent retrieval and augmentation. However, they lack prior decomposition and analysis of the information sources, making this paradigm prone to rigidity and unable to emulate the nuanced trade-offs and reasoning capabilities humans employ when tackling complex problems. Cognitively, human retrieval is guided by task-dependent visual saliency [27], while most retrieval systems rely on monolithic similarity metrics, neglecting essential fine-grained visual anchors [23]. This misalignment necessitates rethinking retrieval paradigms—transitioning from rigid deep learning architectures toward neurocognitively-inspired frameworks that emulate human perceptual dynamics [20].

In recent years, vision foundation models [33, 45] and multimodal foundation models [56] have advanced rapidly, providing us with tools to process, extract, and analyze image information at the sub-image level. Building on the current powerful foundation models and tools, as well as the above insights into the limitations of existing RAG systems, we introduce *Human-Like Retrieval-Augmented Generation (HuLiRAG)*—a retrieval-augmented generation framework designed to emulate the staged dynamics of human perception. Inspired by how the brain incrementally binds referents, parses spatial structure, and reweights evidence in context, our architecture follows a *what–where–reweight* cascade that explicitly aligns memory, attention, and inference with the compositional flow of visual reasoning. HuLiRAG begins with a *Pre-stage*

that employs CLIP [50] to align query semantics with image embeddings, forming a high-recall candidate pool. The subsequent *What* module decomposes each query into open-vocabulary phrases describing objects, attributes, and relations to be localized. These linguistic cues are grounded by the *Where* module, where GroundingDINO [45] predicts region proposals refined by SAM [33] into high-resolution masks, and Alpha-CLIP [56] integrates global and regional representations to compute adaptive similarity weights. Ultimately, the *Reweight* module calibrates the balance between global and local cues through a lightweight, learnable positive–negative optimization, yielding retrieval that is both semantically precise and spatially grounded. Together, these components transform retrieval from a static preprocessing step into an active perceptual loop—grounded, staged, and contextually responsive. We further consolidate this pipeline with a spatially supervised fine-tuning stage that conditions answer generation on SAM-derived masks, ensuring that reasoning remains anchored in visual evidence. Experiments on WebQA [63] and MultimodalQA [57] demonstrate that region-aware reranking and spatial supervision jointly improve factual consistency and referential grounding, enabling language models to “read” images with human-like perceptual structure.

2 Related Work

Retrieval-Augmented Language Models (RALMs). The paradigm of retrieval-augmented language modeling has evolved significantly from early static retrieval architectures that condition generation on a fixed set of passages [22, 36], to more adaptive frameworks featuring differentiable dense retrievers [32], late-interaction encoders for efficient passage scoring [28], and conditional computation strategies that dynamically adjust retrieval cost based on query complexity [4]. Further developments have introduced iterative retrieve–generate loops [30], learned retrieval policies [11], and memory-augmented transformers that support continual external knowledge access [60]. While these methods have greatly improved retrieval efficiency and adaptability in text-based settings, they remain inherently text-centric and thus ill-suited for multimodal reasoning. In particular, they struggle to represent visual concepts that demand fine-grained compositional grounding [26] and fail to adapt retrieval to query-specific cross-modal signals [14], both of which are essential for grounded visual question answering and instance-level image–text retrieval.

Multimodal Retrieval-Augmented Generation. Recent advances in retrieval-augmented generation have extended beyond text-only applications into multimodal settings, where external information retrieval supports vision-language tasks such as VQA, captioning, and instruction following [10, 22, 36]. Core architectures differ in their retrieval strategies: some rely solely on language-based retrieval from text corpora, disregarding the visual context [62]; others embed image-text pairs into joint latent spaces and retrieve based on vector similarity [5, 32, 61], but these representations often entangle semantic and spatial cues in a manner that lacks interpretability [3]. Multi-stage pipelines aim to improve retrieval precision through coarse-to-fine selection and fusion-based reranking [7, 18, 29], and recent work has explored symbolic enhancement [55], multi-hop reranking [44], and the use of multimodal large language models (MLLMs) themselves as rerankers [16].

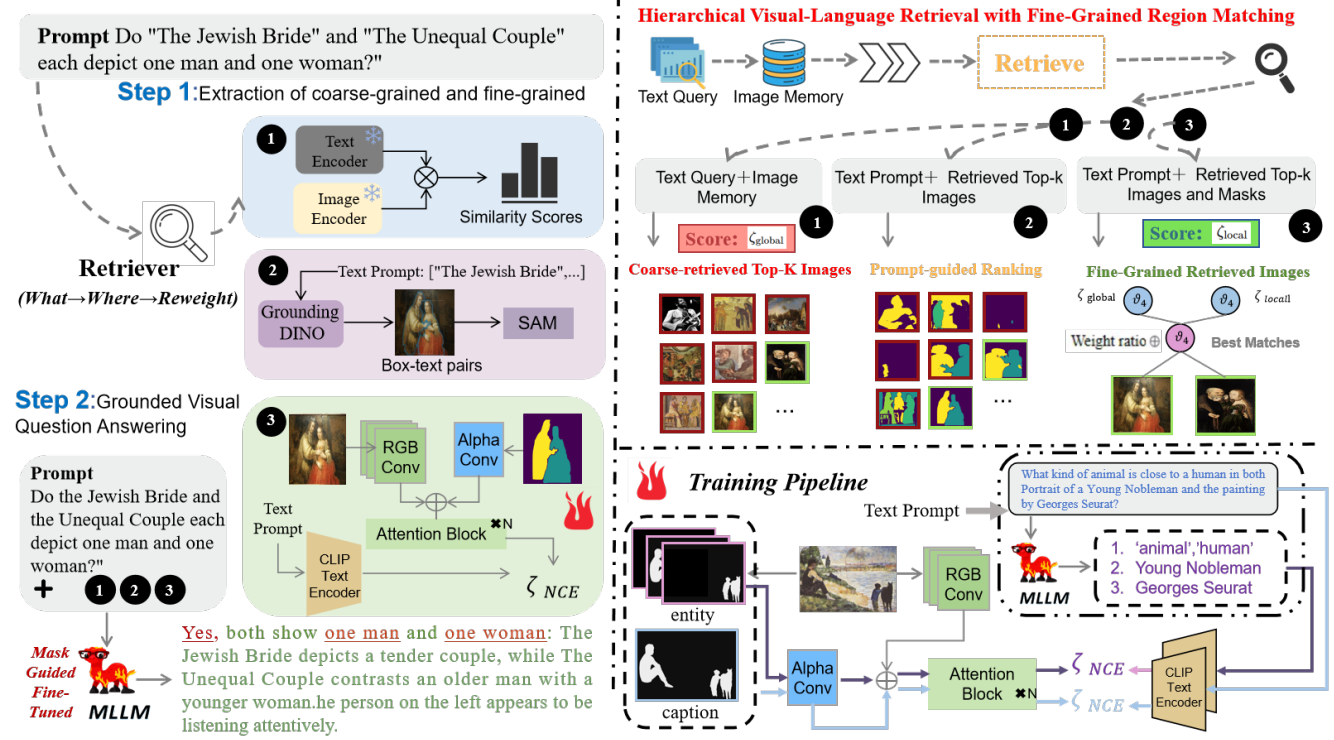


Figure 2: Overview of the HuLiRAG framework. Our method implements a human-like staged retrieval pipeline: (1) global feature matching for candidate shortlisting, (2) query-grounded region refinement via detection and segmentation, and (3) adaptive fusion of global and local cues through a learned weighting scheme. The refined evidence feeds into a grounded VQA module, where Alpha-CLIP jointly optimizes global-local alignment.

Notably, Kosmos-2 [66] adds grounding signals to MLLMs for VQA, but does not directly address staged, region-level reasoning. Despite architectural diversity, most systems treat retrieved content as static evidence—globally conditioned, query-invariant, and aggregated without modeling dynamic, compositional alignment. This design limits the model’s ability to support instance-level reasoning, structured grounding, and flexible adaptation to multimodal query semantics [35, 46, 65]. Our approach therefore reframes retrieval as a neurocognitively staged process rather than enlarging MLLMs themselves.

3 Method

Humans do not retrieve visual informations by processing an image as a single whole. Instead, perception unfolds in stages: a global impression captures the scene, attention narrows to likely regions, and localized cues are weighted before forming a response. This routine of coarse recognition, targeted inspection, and evidence integration underpins our *Human-Like Retrieval-Augmented Generation* (*HuLiRAG*) framework. As shown in Figure 2, HuLiRAG organizes retrieval into a staged pipeline consisting of a pre-stage coarse candidate retrieval (§3.1), which is a typical naive retrieval approach, followed by three modules: *What* for query-to-region decomposition (§3.2), *Where* for visual grounding (§3.3), and *Reweighting*

for adaptive evidence allocation (§3.4). On top of this staged retrieval, we introduce *Spatially-Aware Fine-Tuning with Mask-Guided Supervision* (§3.5), which grounds generation directly in localized evidence. Working in concert, these modules emulate human-like perceptual staging by dynamically binding symbolic queries to spatially grounded visual evidence through a “what–where–reweight–answer” process, enabling compositional and context-sensitive reasoning.

3.1 Pre-stage: Coarse Candidate Retrieval

Before entering the human-like reasoning cascade (*What–Where–Reweighting*), HuLiRAG begins with a *coarse candidate retrieval* step that prunes the visual search space.

We begin retrieval by selecting a compact candidate set that coarsely aligns with the query semantics. Given a query q and an image corpus $\mathcal{I} = \{I_1, \dots, I_N\}$, we adopt frozen CLIP [50] as a dual encoder to compute the text embedding $q_i = E_{\text{text}}(q)$ and the image embeddings $v_i = E_{\text{image}}(I_i)$. Similarity is computed via cosine similarity:

$$s_j^{\text{clip}} = \frac{q_i^T v_j}{\|q_i\| \cdot \|v_j\|}. \quad (1)$$

All image embeddings are pre-indexed with FAISS [31] for scalable retrieval. At inference, we obtain the top- K candidates by:

$$\mathcal{I}_{\text{top}} = \text{TopK}_{I_i \in \mathcal{I}} s_i^{\text{clip}}. \quad (2)$$

In this way, we prune the search space from N to K , while deferring precise grounding and alignment to subsequent modules.

3.2 What: Query-to-Region Decomposition

The second stage of our framework specifies *what* to look for, mirroring the human ability to identify relevant concepts and entities in a question before searching for their spatial locations. Instead of encoding the entire query as a single vector, we decompose it into a set of semantically grounded phrases that delineate the key objects, attributes, and relations to be localized in the next stage. Each query q is first decomposed into an ordered sequence of open-vocabulary phrases $\mathbf{n}(q) = [n_1, \dots, n_k]$, where each n_i denotes a minimal noun phrase with optional modifiers (e.g., “man in blue”, “leftmost sign”, “two cones”). Coreference resolution consolidates repeated mentions, while numerical and spatial cues are explicitly retained, ensuring that $\mathbf{n}(q)$ preserves the fine-grained constraints necessary for subsequent localization. To enhance robustness, phrase construction is regularized to mitigate redundancy and over-fragmentation. We define the lexical representation of a phrase as the lemmatized set of its content words (nouns, adjectives, numerals, and spatial modifiers), extracted via dependency arcs and NP chunking with spaCy [24]. Phrases with substantial lexical overlap are merged:

$$n_i = \begin{cases} n_i, & \text{if } \frac{|V(n_i) \cap V(n_j)|}{|V(n_i) \cup V(n_j)|} \leq 0.7, \\ \text{merge}(n_i, n_j), & \text{otherwise,} \end{cases} \quad (3)$$

where $V(\cdot)$ denotes the lexical set. In addition, repeated mentions are disambiguated by indexing, yielding $n^{(1)}, n^{(2)}, \dots$, so that each textual reference maps uniquely to a visual region.

3.3 Where: From Linguistic Decomposition to Visual Grounding

The second stage of HuLiRAG determines *where* to look and how much to attend within the scene. It bridges linguistic structure and spatial reasoning by grounding textual phrases into visual regions and adaptively allocating their evidential strength. This stage embodies the human-like transition from identifying what entities are described to understanding where they appear and how relevant they are to the question.

3.3.1 Phrase-to-Region Grounding. Each surviving phrase n_k is grounded in the candidate image I_j through a two-step process. GroundingDINO [45] first predicts bounding boxes conditioned on n_k , and we retain only detections with confidence above 0.3, a setting stricter than the default 0.25 to suppress low-quality matches. The Segment Anything Model (SAM) [33] then refines each box b_k into a binary mask m_k using a mask threshold of 0.5, producing sharper region boundaries while maintaining robustness. By associating each n_k with its m_k , we establish explicit phrase-to-region alignments with both semantic fidelity and spatial precision.

The final RGBA patch is constructed as $\tilde{I}_k = I_j \odot m_k$, which preserves the localized structure of the entity while eliminating irrelevant background. This yields a set of clean, phrase-specific patches $\{\tilde{I}_k\}$ that serve as reliable inputs for the adaptive reweighting stage.

3.3.2 Adaptive Evidence Integration. Within the *where* stage, the model further integrates the grounded regions by estimating their relative evidential strength. Pixel-level normalization and semantic feature weighting ensure that salient regions are emphasized while redundant or noisy cues are suppressed, yielding a spatially coherent representation aligned with the query semantics.

Inference. We begin by deriving region weights α_{jk} from soft mask assignments:

$$\alpha_{jk} = \frac{1}{|\Omega(I_j)|} \sum_{p \in \Omega(I_j)} \frac{m_k(p)}{\sum_{l=1}^{T_j} m_l(p) + \epsilon}, \quad (4)$$

where p indexes pixels in the image domain $\Omega(I_j)$, $m_k(p)$ is the binary membership of pixel p in mask m_k , and ϵ avoids division by zero. This formulation enforces a probabilistic partition of the image: overlapping regions share pixels fractionally, and the resulting α_{jk} values sum to unity across regions.

Each masked region \tilde{I}_k is then encoded by Alpha-CLIP into a region embedding r_{jk} , while the query q_m is independently mapped to a text embedding. The overall local relevance of image I_j is computed as a weighted aggregation:

$$s_j^{\text{local}} = \sum_{k=1}^{T_j} \alpha_{jk} \cos(q_m, r_{jk}), \quad (5)$$

where T_j denotes the total number of regions. This inference procedure explicitly links textual phrases to their visual counterparts, while attenuating noisy or overlapping evidence. By construction, reweighting balances fidelity and robustness: salient regions are amplified, redundant regions are down-weighted, and alignment is achieved through a principled fusion of localized evidence.

Training and adaptation. We finetune Alpha-CLIP with a single objective that couples global and regional supervision. For each image I_j with question q and region masks m_k linked to phrases n_k extracted from q , we build two example types: (i) global pairs (I_j, q) to preserve holistic semantics; (ii) regional pairs (\tilde{I}_k, n_k) or (\tilde{I}_k, q) for fine-grained grounding. Formally, the training objective simply sums global and regional contrastive losses:

$$\mathcal{L} = \mathcal{L}_{\text{NCE}}(I_j, q) + \frac{1}{T_j} \sum_{k=1}^{T_j} \mathcal{L}_{\text{NCE}}(\tilde{I}_k, n_k), \quad (6)$$

where \mathcal{L}_{NCE} is the InfoNCE loss applied to both holistic and phrase-grounded pairs. All inputs are resized to a common resolution and tokenized as concatenations of either the phrase or the full query. To accept RGBA inputs, Alpha-CLIP augments the CLIP image encoder with an Alpha Conv branch in the ViT stem; this branch is zero-initialized to keep the RGB path unchanged at warm-up. The text encoder is frozen, deeper transformer layers use a smaller learning rate, and we use hybrid sampling that replaces 10% of regional pairs with full-image queries ($\alpha = 1$) to maintain global understanding.

3.4 Reweight: Adaptive Balance via Positive Negative Sample Pair

CLIP-based joint image–text embeddings offer strong recall but suffer from *semantic myopia*, capturing only gist-level similarity while

blurring fine-grained referents and limiting performance on queries that require localized grounding. At the same time, focusing exclusively on local details overlooks the global context that arises from the interaction among multiple regions. Human perception avoids this limitation by alternating between a holistic understanding of the scene and selective attention to candidate regions.

It is necessary to strike a balance and effectively integrate image-level and subimage-level information. In fact, there are two straightforward strategies to combine global similarity S_{global} and local similarity S_{local} : addition and multiplication.

$$S_{\text{Add}} = S_{\text{global}} + S_{\text{local}}, \quad S_{\text{Multi}} = S_{\text{global}} \cdot S_{\text{local}}. \quad (7)$$

However, both approaches are entirely static—they apply the same fusion rule universally across all retrieval domains and datasets. In reality, different retrieval tasks and datasets inherently exhibit distinct biases. For instance, in medical image retrieval, local similarity is often more critical than global similarity, as pathological lesions are typically small and the organs of interest usually occupy only a small portion of the entire image.

To enhance domain generalization and prevent overfitting to a fixed retrieval bias, we introduce a lightweight calibration stage that adaptively balances global and local similarity after fine-tuning. Instead of relying on a static fusion rule, the final similarity is parameterized as

$$S_{\text{reweight}} = W_g \cdot S_{\text{global}} + W_l \cdot S_{\text{local}} + B, \quad (8)$$

where W_g , W_l , and B are learnable scalar parameters that control the relative contribution of global and local cues.

Since S_{reweight} lacks explicit ground-truth supervision, we employ a positive–negative contrastive formulation to optimize these parameters in a self-calibrating manner. For each query, its ground-truth (GT) image is treated as a positive sample, while a hard negative is drawn from the top five non-GT candidates according to the initial retrieval ranking based on global similarity. The training objective encourages the model to assign a similarity score close to 1 for positive pairs and near 0 for negative pairs, which we implement using a mean squared error (MSE) loss defined as

$$\mathcal{L}_{\text{reweight}} = (1 - S_{\text{reweight}}^+)^2 + (S_{\text{reweight}}^-)^2, \quad (9)$$

where S_{reweight}^+ and S_{reweight}^- denote the reweighted similarity of positive and negative pairs, respectively. This lightweight optimization updates only three scalar parameters (W_g , W_l , and B) while leaving the embedding space intact, enabling HuLiRAG to automatically calibrate the weighting of global and local evidence across heterogeneous retrieval domains.

3.5 Spatially-Aware Fine-Tuning with Mask-Guided Supervision

Although dual-scale reranking strengthens retrieval by combining global and local evidence, the answer generation stage itself remains unconstrained, and the spatial information obtained during the retrieval stage cannot be effectively utilized in the generation stage. As a result, multimodal models may still produce responses that are semantically plausible yet spatially ungrounded, reflecting a persistent gap between retrieval accuracy and reasoning faithfulness. To close this gap, we introduce a spatially supervised fine-tuning

stage that directly anchors the generation process to localized visual evidence. Concretely, we condition the model on both the full image I_j and its masked counterpart $\tilde{I}_k = I_j \odot m_k$, where m_k is the SAM-derived mask obtained from the *where* module of HuLiRAG. Let A^* denote the ground-truth answer. To encourage the generator to utilize both global and localized cues, we randomly drop either I_j or \tilde{I}_k during training, preventing collapse into global-only reasoning. The optimization follows the standard VQA objective:

$$\mathcal{L}_{\text{vqa}} = -\log p(A^* | q, I_j, \tilde{I}_k), \quad (10)$$

and can be further regularized by enforcing prediction consistency between the two visual contexts,

$$\mathcal{L}_{\text{cons}} = \|p(A | q, I_j) - p(A | q, \tilde{I}_k)\|^2, \quad (11)$$

to align predictions across global and masked inputs. Here, $p(A | q, I_j)$ and $p(A | q, I_j \odot m_k)$ denote the predicted probability distributions over the answer space conditioned on the full image I_j or its masked counterpart \tilde{I}_k , respectively, while $\|\cdot\|^2$ denotes the squared Euclidean distance between these two distributions. This encourages the model to remain consistent whether reasoning relies on the full scene or localized evidence. The training objective is defined as $\mathcal{L} = \mathcal{L}_{\text{vqa}} + \mathcal{L}_{\text{cons}}$, directly coupling answer supervision with consistency regularization. By leveraging retrieval-derived masks as anchors, the loss unifies evidence selection and prediction, reinforcing semantic faithfulness, spatial grounding, and overall coherence of the HuLiRAG pipeline.

It's straightforward that during inference, we simultaneously input the full image I_j and the masked image \tilde{I}_k to enhance the model's answer accuracy.

4 Experiments

4.1 Datasets

Experimental Setup. We evaluate our framework on two established benchmarks that stress different aspects of multimodal reasoning: WebQA [63] and MultimodalQA [57]. WebQA comprises over 43,000 real-world image-question-answer triplets harvested from the web, covering diverse domains with long-tail object distributions and noisy visual-textual alignment. In contrast, MultimodalQA features 29,918 questions grounded in complex tabular visual contexts, requiring multi-hop reasoning over structured spatial layouts.

For evaluation, we adopt two complementary protocols. In the retrieval stage, we measure performance with Recall@K ($K=1, 5, 10$) [50, 63], which assesses whether the ground-truth image is successfully ranked within the top- K candidates. For VQA, we adopt Exact Match (EM) on MultimodalQA, token-level F1 on WebQA, and additionally employ the LLM-as-a-Judge protocol as a complementary assessment of answer quality. These combined metrics provide a holistic evaluation of retrieval precision and reasoning fidelity.

Implementation Details. All experiments are conducted on a cluster with 8×NVIDIA H20 GPUs, using FP16 mixed-precision training. For MultimodalQA [57], the official test split does not release answer labels; following prior work [16], we therefore use the development set as the evaluation benchmark. For WebQA [63], which similarly lacks an annotated test set, we adopt the common 8:1:1 random split into training/validation/test subsets, consistent

Table 1: Recall performance (R@k) on MMQA and WebQA. “Backbone (Vanilla)” denotes raw retrieval with the base retriever presented in Section 3.1, while “+HuLiRAG-Ret” denotes the same retriever augmented with our reranking module (AlphaCLIP included in the module is fine-tuned.) presented in Section 3.2-3.4. Note: this table reports retrieval-only results, without the generation stage.

Retriever Backbone	MMQA						WebQA					
	Vanilla			+HuLiRAG-Ret			Vanilla			+HuLiRAG-Ret		
	R@1	R@5	R@10	R@1	R@5	R@10	R@2	R@5	R@10	R@2	R@5	R@10
Clip-ViT-L/14@336px	79.13	88.26	90.97	87.57	93.63	96.95	58.37	73.52	86.74	73.41	82.80	88.26
-Finetuned	77.66	88.17	90.21	86.71	93.30	96.38	57.76	74.77	85.70	71.38	83.23	86.64
AlphaClip-(Full-mask)	45.35	66.09	75.22	54.52	73.39	82.97	44.33	71.51	80.14	52.05	79.95	83.57
-Finetuned	49.86	72.48	80.19	59.20	79.35	86.83	48.28	73.64	83.53	57.30	82.51	87.03
Vis-BGE-base	46.52	70.87	78.26	75.25	87.03	90.14	29.15	48.23	59.46	53.22	59.31	66.71
Vis-BGE-m3	41.30	64.78	69.57	72.96	87.91	92.36	26.84	46.56	57.51	50.76	57.24	64.97
InternVL-C	78.22	90.61	94.04	88.56	94.78	97.09	65.22	81.93	88.31	83.25	89.89	91.57
InternVL-G	78.91	90.52	94.83	87.32	94.41	97.24	65.17	80.52	88.33	81.85	87.62	90.98

Table 2: Retrieval performance of HuLiRAG-Ret across global, local, and fused similarity strategies. The “Global” and “Local” levels represent retrieval using only holistic or region-aware similarity without cross-scale fusion, whereas the other strategies fuse the two through addition, multiplication, or a learnable reweighting mechanism.

Strategy	MMQA R@1	WebQA R@2	WebQA R@10
Global level	77.66	57.76	85.70
Local level	83.83	67.32	86.14
Addition	86.04	70.45	86.33
Multiply	86.19	70.50	86.38
Learnable Reweight	86.71	71.38	86.64

with recent practice [17, 70]. All images are resized to 336×336 pixels. During inference, the latency of CLIP-based global retrieval is 1.4 seconds per sample, and dual-scale reranking latency is 4.9 seconds per sample.

We implement a two-path RAG pipeline with global retrieval using CLIP-ViT-L/14@336px [50] and local alignment via Alpha-CLIP with an RGBA branch. Training employs InfoNCE with AdamW (weight decay 0.01), cosine-annealed learning rates, large batches (1024 for CLIP, 512 for Alpha-CLIP), and mixed precision; early stopping is triggered by validation R@1 (patience = 5). At inference, CLIP retrieves the top-20 candidates, which are reranked by Alpha-CLIP and reduced to top-N (N = 2 for WebQA, N = 1 for MultimodalQA). Across this pipeline, we benchmark InternVL and LLaVA backbones [43, 59, 75] under three regimes: frozen, standard finetuning, and our Mask-Guided Finetuning, demonstrating consistent VQA gains across model scales.

4.2 Main Results

Fine-grained regional alignment via HuLiRAG delivers consistent and significant retrieval efficacy enhancements. As

shown in Table 1, the integration of HuLiRAG substantially improves reranking performance beyond vanilla retrieval across MMQA and WebQA benchmarks. For the widely adopted CLIP-ViT-L/14@336px backbone, MMQA R@1 increases from 79.13% to 87.57%, while WebQA R@2 improves from 58.37% to 73.41%. Interestingly, the finetuned variant performs slightly worse than the vanilla backbone, suggesting that task-specific adaptation may aggravate overfitting to Internet-scale pretraining data and thus reduce cross-dataset generalization, leaving HuLiRAG to partly restore the gap. In contrast, AlphaCLIP under a full mask regime, where the entire image is uniformly treated as foreground without selective focus, starts from much weaker baselines (45.35% R@1 on MMQA, 44.33% R@2 on WebQA), yet still shows strong recovery once paired with HuLiRAG. Beyond CLIP style encoders, the framework consistently enhances Vis-BGE and InternVL families, with Vis-BGE-base gaining +28.73 on MMQA R@1 and +24.07 on WebQA R@2, and InternVL-C advancing to 97.09% R@10 on MMQA and 83.25% R@2 on WebQA. Notably, relative improvements are largest on weaker retrievers such as Vis-BGE-m3, while top tier systems like InternVL-G still yield non-trivial gains.

Main VQA Results. Table 3 shows that our HuLiRAG pipeline consistently improves performance across MMQA and WebQA. On MMQA, InternVL-1B improves from 30.00 to 41.14 EM with HuLiRAG, recovering 53% of the gap toward its GT oracle (50.56), with larger backbones exhibiting comparable recovery ratios. Since MMQA primarily evaluates short, factoid-style answers, EM is the natural metric. On WebQA, which involves longer free-form responses, HuLiRAG consistently adds 3%–6% F1 over the CLIP→VQA baseline, and the gains persist across scales. Within HuLiRAG, the proposed Mask-Guided FT yields an additional 0.4%–3.5% absolute improvement, indicating that domain-aware supervision not only strengthens retrieval gains but also mitigates instability. Although introduced here as part of HuLiRAG, this lightweight mechanism is transferable and can be seamlessly applied to fine-tuning other LLM backbones for VQA where region-aware signals are advantageous. These findings clarify that HuLiRAG equipped with Mask-Guided

Table 3: EM (%) on MultimodalQA and F1 (%) on WebQA across inference settings. Text-only: question only; CLIP→VQA: retrieval+VQA; HuLiRAG: cascade method; Ground-truth Image (oracle setting with gold-standard image directly given). Symbols: \circ Zero-shot, \blacktriangle Finetuned, \blacksquare Mask-Guided FT.

Model	Regime	MultimodalQA (EM, %)				WebQA (F1, %)		
		Text-only	CLIP→VQA	HuLiRAG	GT Image	CLIP→VQA	HuLiRAG	GT Image
InternVL-1B	\circ Zero-shot	12.17	30.00	41.14	50.56	39.32	43.79	45.85
	\blacktriangle Finetuned	21.74	55.22	57.46	61.93	71.94	72.87	75.05
	\blacksquare Mask-Guided FT	22.81	55.73	59.35	63.84	72.82	74.21	76.79
InternVL-2B	\circ Zero-shot	17.39	47.39	50.37	52.29	43.75	49.76	51.22
	\blacktriangle Finetuned	24.78	57.39	61.47	64.39	72.81	74.88	76.95
	\blacksquare Mask-Guided FT	26.03	58.66	63.16	66.26	74.15	76.27	78.53
InternVL-4B	\circ Zero-shot	29.13	50.00	52.93	55.96	50.21	53.58	56.94
	\blacktriangle Finetuned	32.17	61.74	65.17	69.27	76.82	77.49	78.07
	\blacksquare Mask-Guided FT	34.66	63.11	67.52	72.35	77.75	79.45	80.20
InternVL-8B	\circ Zero-shot	34.35	53.48	55.96	58.72	44.13	47.77	51.28
	\blacktriangle Finetuned	36.61	67.10	71.04	75.97	74.34	75.89	77.08
	\blacksquare Mask-Guided FT	39.43	69.57	74.31	79.88	75.72	77.38	78.84

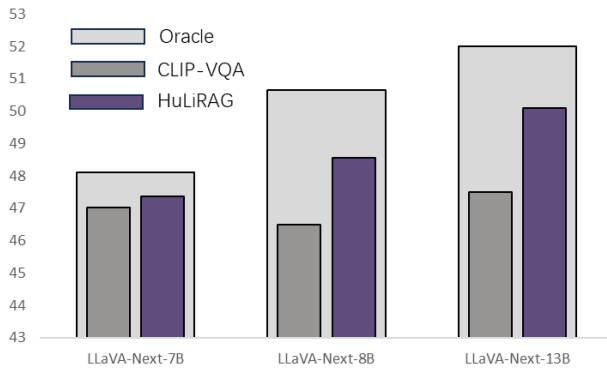


Figure 3: Evaluating LLaVA-Next (7B/8B/13B) with CLIP→VQA, HuLiRAG, and Oracle under the LLM-as-a-Judge protocol.

FT not only narrows the gap toward oracle performance but also provides a broadly applicable strategy for stabilizing and amplifying retrieval-based VQA.

To complement the InternVL results, we further benchmark the LLaVA-Next family (7B, 8B, 13B) under our retrieval settings. Unlike WebQA F1, which may conflate retrieval accuracy with scaling effects of large models, we adopt the LLM-as-a-Judge protocol [72] based on MT-Bench and Chatbot Arena. Using the fixed single-answer grading prompt (shown in Table 5), we employ GPT-4 as the judging model to score each response, and compare CLIP→VQA, our HuLiRAG pipeline, and the GT-Image oracle. As shown in Fig. 3, HuLiRAG consistently improves over CLIP→VQA across all scales, closely tracking the oracle even at 7B, and narrowing the gap further at 8B and 13B (e.g., on LLaVA-Next-13B HuLiRAG reduces more than half of the gap to the oracle).

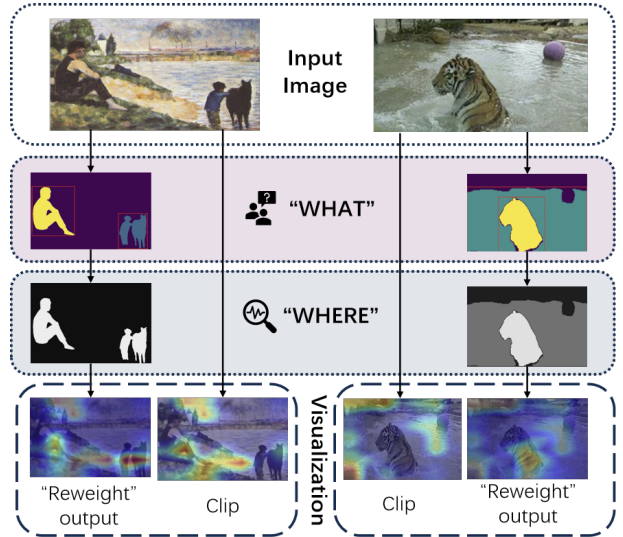


Figure 4: Comparison between CLIP’s global attention (query-agnostic) and HuLiRAG’s *What-Where-Reweight* mechanism (query-conditioned). HuLiRAG mimics human perception by adaptively fusing global context with masked local regions. The HuLiRAG heatmaps are obtained by overlaying regional relevance on top of CLIP’s original activation, showing how adaptive fusion sharpens attention to query-relevant evidence.

We further evaluate with Qwen [8] and GPT4o[2] as answer generators, while DeepSeek [40] serves as the judge. In addition to EM and F1, DeepSeek assigns a holistic Score on a 0–10 scale, following a rubric that weighs helpfulness, accuracy, depth, and

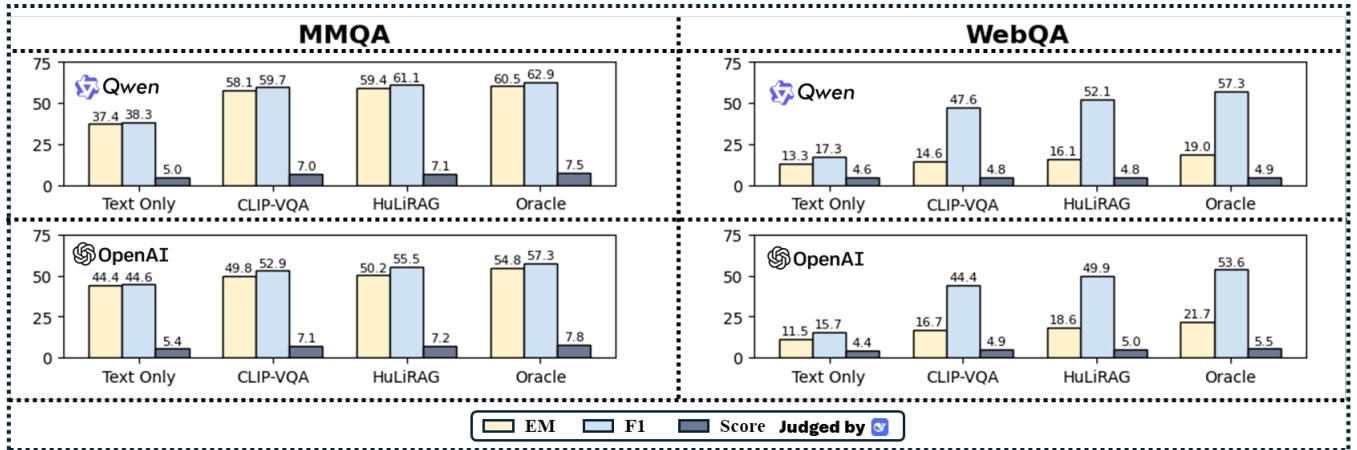


Figure 5: Evaluation by business LLM

Table 4: Ablation of HuLiRAG components on MMQA and WebQA.

Variant	MMQA R@1	WebQA F1
Full HuLiRAG	87.57	76.79
w/o What	70.38	63.52
w/o Where	79.53	70.16
w/o Reweighting	86.04	75.15

clarity. The detailed criteria for this scoring protocol are summarized in Table 6. As shown in Figure 5, HuLiRAG consistently raises judged quality across MMQA and WebQA, moving closer to the oracle. For instance, on MMQA with Qwen as the generator, HuLiRAG improves the judged Score from 6.98 (CLIP→VQA) to 7.11, approaching the oracle level of 7.45.

4.3 Analysis

Refinement Study: Effect of Fusion Strategies. Table 2 reports the effect of different similarity fusion strategies in HuLiRAG-Ret. Global and local levels serve as reference points that rely solely on holistic or region-aware similarity without any fusion. All fusion strategies yield clear improvements, confirming the benefit of combining the two. Addition performs simple linear blending, offering moderate gains (MMQA R@1: 85.83→86.04). Multiply further enhances precision by emphasizing regions where both cues are strong (MMQA R@1: 86.19, WebQA R@2: 70.50). Learnable Reweighting achieves the best overall performance (MMQA R@1: 86.71, WebQA R@2: 71.38, WebQA R@10: 86.64), as it adaptively calibrates the contributions of global and local similarity through a lightweight parameterized fusion. These results highlight that adaptive weighting provides the most balanced and discriminative retrieval alignment.

Visual Cognitive Pipeline: Emulating Expert Reasoning. For queries requiring multi-layered understanding (e.g., “What kind of animal is close to a human in Seurat’s painting and *Portrait of a Young Nobleman*?”), our architecture follows a three-stage pipeline

(Figure 4) that surpasses conventional models trapped by global feature homogenization. The “WHAT” stage localizes entities using open-vocabulary prompts and region masks, for instance localizing the child and dog in Seurat’s painting while minimizing the influence of the seated figure. The “WHERE” stage then disentangles spatial relations via binary masks, enabling fine-grained reasoning such as separating a tiger’s contour from rippling water where CLIP conflates “tiger” with “aquatic context.” Finally, the “Reweighting” stage shifts attention toward interaction zones, concentrating on task-relevant regions like the tiger’s body, while CLIP disperses activation over distractors. This pipeline, instantiated in HuLiRAG’s design, systematically integrates global context with localized evidence, ensuring reasoning that is both semantically faithful and spatially grounded. By emulating expert workflows that begin with global composition and proceed to fine-grained inspection, the framework avoids shallow feature matching and instead produces structured, query-relevant reasoning that generalizes across diverse domains.

Component Analysis. We further analyze the contributions of HuLiRAG’s stages in Table 4. The *what* stage is essential because it anchors free-form textual queries to visual referents and decomposes them into grounded entities that guide SAM and Alpha-CLIP for localized alignment. Without it, the model feeds the entire sentence directly to SAM for segmentation, producing coarse and semantically inconsistent regions that are later encoded by Alpha-CLIP, leading to severe semantic drift (MMQA R@1: 72.1, WebQA F1: 65.1). Removing the *where* stage disables spatial grounding by replacing GroundingDINO and SAM with a full-image mask, collapsing reranking into a global comparison between CLIP and Alpha-CLIP embeddings and causing a notable drop in precision (MMQA R@1: 79.5, WebQA F1: 70.1). Discarding the *reweight* stage retains both global and local cues but fuses them linearly, reducing adaptivity and discriminative strength (MMQA R@1: 86.0, WebQA F1: 75.2). In addition to the three stages, mask-guided fine-tuning, though introduced as part of HuLiRAG, constitutes a general mechanism for enforcing spatial grounding: across scales, it consistently improves retrieval-augmented VQA (e.g., InternVL-2B EM: 65.0→69.0;

WebQA F1: 74.9→77.6), underscoring both its robustness and generality.

5 Conclusion

In this work, we introduced Human-Like Retrieval-Augmented Generation (HuLiRAG), a cognitively inspired framework that overcomes static global-only retrieval. Through a *what-where-reweight* mechanism, HuLiRAG grounds queries in fine-grained visual evidence by integrating objects, relations, and semantics. This design reflects human perceptual reasoning, adaptively balancing global context with local details. Experiments on WebQA and MultimodalQA show consistent gains in retrieval precision and answer consistency, underscoring that cognitively motivated architectures can improve both interpretability and performance in multimodal reasoning.

References

- [1] Mohammad Mahdi Abootorabi, Amirhosein Zobeiri, Mahdi Dehghani, Mohammadi Mohammadi, Bardia Mohammadi, Omid Ghahroodi, Mahdieh Soleymani Baghshah, and Ehsaneddin Asgari. 2025. Ask in Any Modality: A Comprehensive Survey on Multimodal Retrieval-Augmented Generation. *arXiv preprint arXiv:XXXX.XXXX* (2025). Submitted for publication.
- [2] Josh Achiam, Steven Adler, Sandhini Agarwal, Lama Ahmad, Ilge Akkaya, Florencia Leoni Aleman, Diogo Almeida, Janko Altenschmidt, Sam Altman, Shyamal Anadkat, et al. 2023. Gpt-4 technical report. *arXiv preprint arXiv:2303.08774* (2023).
- [3] Chaitanya Aggarwal, Yash Sharma, and et al. 2024. ImageBind: One Embedding Space to Bind Them All. *arXiv preprint arXiv:2305.05665* (2024).
- [4] Joshua Ainslie, Minghua Deng, and et al. 2023. Conditional Computation in Large Language Models via Mixture-of-Experts Retrieval. In *ACL Findings*.
- [5] Jean-Baptiste Alayrac, Jeff Donahue, Paul Luc, Antoine Miech, Ian Barr, Ali Hassani, Arthur Mensch, Katie Millican, Luyu Reynolds, Roman Ring, et al. 2022. Flamingo: A Visual Language Model for Few-Shot Learning. In *Advances in Neural Information Processing Systems*.
- [6] Anthropic. 2023. Claude 3 Opus. (2023).
- [7] Akari Asai, Kazuma Hashimoto, Hannaneh Hajishirzi, Richard Socher, and Caiming Xiong. 2020. Learning to Retrieve Reasoning Paths over Wikipedia Graph for Question Answering. In *ACL*.
- [8] Yujia Bai, Jingsong Zhang, Shuai Li, Yifan Zhang, Fei Xue, Xiaoyu Zhu, Yan Zhao, et al. 2023. Qwen-VL: A Versatile Vision-Language Model for Understanding, Localization, Text Reading, and Beyond. *arXiv preprint arXiv:2309.11271* (2023).
- [9] Seungju Bang, Yuxin Xie, Wonjae Lee, Min Song, Jaehong Kim, Jihoon Kang, and Nojun Kwak. 2023. A Multimodal Perspective: A Survey of Recent Advances in Foundation Models. *arXiv:2309.10020* (2023).
- [10] Sebastian Borgeaud, Arthur Mensch, Jordan Hoffmann, and et al. 2022. Improving language models by retrieving from trillions of tokens. *Nature* (2022).
- [11] Sebastian Borgeaud, Arthur Mensch, Jordan Hoffmann, and et al. 2023. Improving Language Models by Retrieving from Trillions of Tokens. In *International Conference on Learning Representations (ICLR)*.
- [12] Nicolas Carion, Francisco Massa, Gabriel Synnaeve, Nicolas Usunier, Alexander Kirillov, and Sergey Zagoruyko. 2020. End-to-end object detection with transformers. *ECCV* (2020).
- [13] Xi Chen, Xiao Wang, Bolei Zhou, Yue Lin, Qi Zhang, Zhuang Liu, and Han Hu. 2023. PaLI: A Jointly-Scaled Multilingual Language-Image Model. *ICLR* (2023).
- [14] Xudong Chen, Fan Yang, Peng Wang, and et al. 2022. Dynamic Cross-Modal Retrieval with Query-Specific Adaptation. In *European Conference on Computer Vision (ECCV)*.
- [15] Y. Chen and L. Wang. 2024. Granularity Limitations in Entity-Grounded Multimodal Retrieval. *Transactions of the Association for Computational Linguistics* 12 (2024), 789–805.
- [16] Zhanpeng Chen, Chengjin Xu, Yiyuan Qi, and Jian Guo. 2024. Mllm is a strong reranker: Advancing multimodal retrieval-augmented generation via knowledge-enhanced reranking and noise-injected training. *arXiv preprint arXiv:2407.21439* (2024).
- [17] Xiang Dai et al. 2023. InternVL: Multimodal Pretraining with Frozen Vision and Language Models. In *ICLR*.
- [18] Xueyan Dai and et al. 2023. InstructBLIP: Towards General-purpose Vision-Language Models with Instruction Tuning. *arXiv preprint arXiv:2305.06500* (2023).
- [19] Google DeepMind. 2023. Gemini: A Family of Highly Capable Multimodal Models. *arXiv preprint arXiv:2312.11805* (2023).
- [20] S.J. Gershman and N.D. Daw. 2024. Neurocognitive Foundations of Dynamic Information Retrieval. *Trends in Cognitive Sciences* 28, 3 (2024), 189–205.
- [21] Ruiqi Guo, Philip Sun, Erik Lindgren, Quan Geng, David Simcha, Felix Chern, and Sanjiv Kumar. 2020. Accelerating Large-Scale Inference with Anisotropic Vector Quantization. In *ICML*.
- [22] K. Guu and et al. 2020. REALM: Retrieval-Augmented Language Model Pre-Training. *Proceedings of ACL* (2020). <https://arxiv.org/abs/2002.08909>
- [23] S. Hochstein and M. Ahissar. 2023. Visual Anchoring in Compositional Reasoning. In *Proceedings of the Annual Meeting of the Cognitive Science Society*. 1128–1134.
- [24] Matthew Honnibal. 2017. spaCy 2: Natural language understanding with Bloom embeddings, convolutional neural networks and incremental parsing. (*No Title*) (2017).
- [25] Drew A Hudson and Christopher D Manning. 2018. Compositional attention networks for machine reasoning. *ICLR* (2018).
- [26] Drew A Hudson and Christopher D Manning. 2019. GQA: A New Dataset for Real-World Visual Reasoning and Compositional Question Answering. In *Proceedings of the IEEE Conference on Computer Vision and Pattern Recognition*. 6700–6709.
- [27] L. Itti and A. Borji. 2024. Task-Contingent Visual Saliency Modulation. *IEEE Transactions on Pattern Analysis and Machine Intelligence* 46, 1 (2024), 287–301.
- [28] Gautier Izacard, Fabio Petroni, and et al. 2022. A Late-Interaction Retriever for Open-Domain Question Answering. In *International Conference on Learning Representations (ICLR)*.
- [29] Gautier Izacard and Sebastian Riedel. 2022. Few-Shot Learning with Retrieval-Augmented Language Models. In *NeurIPS*.
- [30] Jing Jiang, Ruiqi Zhong, and et al. 2023. Iterative Retrieval-Generation for Knowledge-Intensive Tasks. In *EMNLP*.
- [31] Jeff Johnson, Matthijs Douze, and Hervé Jégou. 2021. Billion-Scale Similarity Search with GPUs. In *IEEE Transactions on Big Data*, Vol. 7. IEEE, 535–547. doi:10.1109/TBDB.2019.2921572
- [32] Vladimir Karpukhin, Barlas Oğuz, Sewon Min, Patrick Lewis, and et al. 2020. Dense Passage Retrieval for Open-Domain Question Answering. In *Empirical Methods in Natural Language Processing (EMNLP)*.
- [33] Alexander Kirillov et al. 2023. Segment Anything. *arXiv preprint arXiv:2304.02643* (2023).
- [34] S.M. Kosslyn. 2023. *Mental Imagery in Cognitive Processes*. MIT Press, Cambridge, MA.
- [35] Stephen M. Kosslyn, William L. Thompson, and Giorgio Ganis. 2003. *The Case for Mental Imagery*. Oxford University Press.
- [36] Patrick Lewis, Ethan Perez, Aleksandra Piktus, and et al. 2020. Retrieval-Augmented Generation for Knowledge-Intensive NLP. In *Advances in Neural Information Processing Systems (NeurIPS)*.
- [37] Junnan Li, Dongxu Li, Caiming Xiong, and Steven Hoi. 2022. BLIP: Bootstrapping Language-Image Pre-training for Unified Vision-Language Understanding and Generation. In *ICML*.
- [38] Weizhe Lin, Jinghong Chen, Jingbiao Mei, Alexandru Coca, and Bill Byrne. 2023. Fine-grained late-interaction multi-modal retrieval for retrieval augmented visual question answering. *Advances in Neural Information Processing Systems* 36 (2023), 22820–22840.
- [39] Weizhe Lin, Jingbiao Mei, Jinghong Chen, and Bill Byrne. 2024. Preflmr: Scaling up fine-grained late-interaction multi-modal retrievers. *arXiv preprint arXiv:2402.08327* (2024).
- [40] Aixin Liu, Bei Feng, Bing Xue, Bingxuan Wang, Bochao Wu, Chengda Lu, Chenggang Zhao, Chengqi Deng, Chenyu Zhang, Chong Ruan, et al. 2024. Deepseek-v3 technical report. *arXiv preprint arXiv:2412.19437* (2024).
- [41] Fangyu Liu, Daniel Vandyke, Nigel Collier, Phil Wang, Ivan Vulić, and Anna Korhonen. 2024. Multimodal Foundation Models: From Specialists to General-Purpose Assistants. *Foundations and Trends in Computer Graphics and Vision* (2024).
- [42] Haotian Liu, Chunyuan Zhang, Yutong Xu, Faisal Zhang, and Jianfeng Gao. 2023. Visual instruction tuning. In *Advances in Neural Information Processing Systems (NeurIPS)*.
- [43] Haotian Liu, Chunyuan Zhang, Yutong Zhang, Yifan Xu, Yuxin Shen, Petros Maniatis, Jianfeng Wang, Jiasi Yang, Hao Tang, Ming Zeng, et al. 2024. LLaVA-1.5: Improving Language-Vision Alignment with GPT-4. *arXiv preprint arXiv:2401.06018* (2024).
- [44] Shenyang Liu et al. 2024. mR²AG: Multi-Agent Reflective Retrieval-Augmented Generation. *arXiv preprint arXiv:2411.15041* (2024).
- [45] Shilong Liu, Zhaoyang Zhang, Yujie Zhang, Feng Wang, Xiyang Chen, Hao Zhang, Xinlong Wang, Yue Cao, Han Hu, and Stephen Lin. 2023. Grounding DINO: Marrying DINO with grounded pre-training for open-set object detection. *arXiv preprint arXiv:2303.05499* (2023).
- [46] Jiayuan Mao, Tete Xiao, Yuning Jiang, Jian Sun, Zhou Yu, and Yuning Jiang. 2019. Counterfactual VQA: A Cause-Effect Look at Language Bias. In *CVPR*.
- [47] Thomas Mensink, Jasper Uijlings, Lluís Castrejón, Arushi Goel, Felipe Cadar, Howard Zhou, Fei Sha, André Araujo, and Vittorio Ferrari. 2023. Encyclopedic vqa: Visual questions about detailed properties of fine-grained categories. In *Proceedings of the IEEE/CVF International Conference on Computer Vision*. 3113–3124.

- [48] E.K. Miller, J. Duncan, and T.J. Buschman. 2023. Dynamic Multi-Granular Integration in Human Visual Processing. *Nature Neuroscience* 26, 7 (2023), 1027–1039.
- [49] OpenAI. 2023. GPT-4 Technical Report. *arXiv:2303.08774* (2023).
- [50] Alec Radford, Jong Wook Kim, Christopher Hallacy, Aditya Ramesh, Gabriel Goh, Sandhini Agarwal, Girish Sastry, Amanda Askell, Pamela Mishkin, Jack Clark, et al. 2021. Learning transferable visual models from natural language supervision. *International Conference on Machine Learning* (2021).
- [51] Alec Radford, Jong Wook Kim, Chris Hallacy, Aditya Ramesh, Gabriel Goh, Sandhini Agarwal, Girish Sastry, Amanda Askell, Phil Mishkin, Jack Clark, et al. 2021. Learning Transferable Visual Models From Natural Language Supervision. In *ICML*.
- [52] Vipula Rawte, Amit Sheth, and Amitava Das. 2023. Survey of Hallucination in Natural Language Generation. *Comput. Surveys* (2023).
- [53] Shaoqing Ren, Kaiming He, Ross Girshick, and Jian Sun. 2015. Faster r-cnn: Towards real-time object detection with region proposal networks. *NeurIPS* (2015).
- [54] Anna Rohrbach, Lisa Anne Hendricks, Kaylee Burns, Trevor Darrell, and Kate Saenko. 2018. Object Hallucination in Image Captioning. *EMNLP* (2018).
- [55] Yilun Shen, Zhaojiang Zhou, Yingwei Luo, Yiqin Wang, Xiangning Lin, and Yang Liu. 2024. MM-K-RAG: Multimodal Knowledge Retrieval-Augmented Generation for Open-Domain VQA. *arXiv preprint arXiv:2402.09768* (2024).
- [56] Zeyi Sun, Ye Fang, Tong Wu, Pan Zhang, Yuhang Zang, Shu Kong, Yuanjun Xiong, Dahua Lin, and Jiaqi Wang. 2024. Alpha-clip: A clip model focusing on wherever you want. In *Proceedings of the IEEE/CVF conference on computer vision and pattern recognition*. 13019–13029.
- [57] Alon Talmor, Jonathan Herzig, Robin Jia, Jonathan Berant, and Eunsol Choi. 2021. MultimodalQA: Complex Question Answering over Text, Tables and Images. In *NAACL*.
- [58] Ashish Vaswani, Noam Shazeer, Niki Parmar, Jakob Uszkoreit, Llion Jones, Aidan N Gomez, Łukasz Kaiser, and Illia Polosukhin. 2017. Attention is all you need. *NeurIPS* (2017).
- [59] Wenhui Wang, Li Dong, Zhiyi Yu, Can Xu, Shuming Huang, Qing Ye, Weizhen Chen, Rui Cao, Ziyang Sun, Songhao Zhang, Yeyun Gong, and Furu Wei. 2025. InternVL3.5: Advancing Open-Source Multimodal Models in Versatility, Reasoning, and Efficiency. *arXiv preprint arXiv:2508.18265* (2025).
- [60] Tongshuang Wu, Luyu Gao, and et al. 2022. Memorizing Transformers. In *Advances in Neural Information Processing Systems (NeurIPS)*.
- [61] Wenhui Xiong and et al. 2021. Answering Complex Open-Domain Questions with Multi-Hop Dense Retrieval. In *International Conference on Learning Representations (ICLR)*.
- [62] Ruiyang Yang, Linjie Li, and et al. 2023. Multimodal RAG: Towards Retrieval-Augmented Multimodal LLMs. *arXiv preprint arXiv:2308.12966* (2023).
- [63] Weijia Yang et al. 2022. WebQA: Multihop and multimodal open-domain question answering. *arXiv preprint arXiv:2201.12086* (2022).
- [64] Michihiro Yasunaga, Hongyu Ren, Antoine Bosselut, Percy Liang, and Jure Leskovec. 2023. RA-CM3: Retrieval-Augmented Multimodal Language Modeling with Knowledge Distillation. In *ICLR*.
- [65] Rowan Zellers, Ximing Lu, and et al. 2022. MERLOT Reserve: Neural Script Knowledge through Vision and Language and Sound. In *CVPR*.
- [66] Chenfei Zhang, Xiyang Li, Xizhou Hu, Wenhui Dai, Ze Yang, Zhilin Liu, Han Wang, Hongyang Li, Dahua Lin, Jianfeng Wang, et al. 2023. Kosmos-2: Grounding Multimodal Large Language Models to the World. *arXiv preprint arXiv:2306.14824* (2023).
- [67] Youcai Zhang, Jinyue Huang, and Liang Ding. 2023. Multimodal Large Language Models: A Survey. *arXiv:2306.13549* (2023).
- [68] Yu Zhang, Zheng Liu, Tianyi Zhou, and Danqi Chen. 2024. Precision Filtering for Retrieval-Augmented Generation. In *NAACL*.
- [69] Yifan Zhang, Jing Wang, Zhe Chen, and Furong Huang. 2024. Graph-Based Approximate Nearest Neighbor Search for Multimodal Retrieval. In *AAAI*.
- [70] Zhuosheng Zhang, Haiyang Li, Qiang Liu, Hai Zhao, and Zuchao Lin. 2023. Multimodal Chain-of-Thought Reasoning in Language Models. In *Proceedings of the 61st Annual Meeting of the Association for Computational Linguistics (ACL)*. 2528–2544.
- [71] Zhengxuan Zhang, Yin Wu, Yuyu Luo, and Nan Tang. 2025. Fine-Grained Retrieval-Augmented Generation for Visual Question Answering. *arXiv preprint arXiv:2502.20964* (2025).
- [72] Lianmin Zheng, Wei-Lin Chiang, Ying Sheng, Siyuan Zhuang, Zhanghao Wu, Yonghao Zhuang, Zi Lin, Zhuohan Li, Dacheng Li, Eric Xing, et al. 2023. Judging llm-as-a-judge with mt-bench and chatbot arena. *Advances in neural information processing systems* 36 (2023), 46595–46623.
- [73] Bowen Zhou et al. 2023. Detecting and Preventing Hallucinations in Large Vision Language Models. *arXiv preprint arXiv:2308.05837* (2023).
- [74] B. Zhou, C. Rudin, and K. Yu. 2024. Explainability Bottlenecks in Multimodal Embedding Spaces. In *Proceedings of the ACL*. 2205–2220.
- [75] Wan Zhu, Li Dong, Zhiyi Yu, Can Xu, Wenhui Wang, Shuming Huang, Qing Ye, Weizhen Chen, Rui Cao, Ziyang Sun, Songhao Zhang, Yeyun Gong, and Furu Wei. 2025. InternVL3: Exploring Advanced Training and Test-Time Recipes for Open-Source Multimodal Models. *arXiv preprint arXiv:2504.10479* (2025).

Table 5: Evaluation instructions for the judging system.

System Instruction	
Prompt	<p>Please act as an impartial judge and evaluate the quality of the response provided by an AI assistant to the user question displayed below. Your evaluation should consider factors such as the helpfulness, relevance, accuracy, depth, creativity, and level of detail of the response.</p> <p>Begin your evaluation by providing a short explanation. Be as objective as possible. After providing your explanation, please rate the response on a scale of 1 to 100, where only integer scores are allowed, by strictly following this format: "Rating: [[X]]", for example: "Rating: [[85]]".</p>
Format	<p>[Question] {question} [The Start of Assistant's Answer] {answer} [The End of Assistant's Answer]</p>

Table 6: Extended evaluation rubric showing detailed criteria (Helpfulness, Accuracy, Depth, Clarity) with weights, ranges, and scoring rules.

Evaluation Criteria (1–10 scale, weighted)	
Helpfulness (0.35)	<p>Measures whether the answer resolves the user's intent with actionable, directly useful content.</p> <p>1–3: Misses intent or irrelevant.</p> <p>4–6: Partial resolution with significant gaps.</p> <p>7–8: Good coverage, minor omissions.</p> <p>9–10: Fully actionable, comprehensive, anticipates implicit needs.</p>
Accuracy (0.35)	<p>Captures factual correctness and avoidance of misleading claims.</p> <p>1–3: Major errors or hallucinations.</p> <p>4–6: Noticeable inaccuracies or overgeneralizations.</p> <p>7–8: Mostly accurate with minor issues.</p> <p>9–10: Perfectly accurate, with explicit handling of uncertainty.</p>
Depth (0.20)	<p>Evaluates reasoning structure and completeness.</p> <p>1–3: Extremely superficial, no reasoning.</p> <p>4–6: Minimal reasoning, key steps missing.</p> <p>7–8: Solid explanation, but shallow in scope.</p> <p>9–10: Thorough, structured, anticipates edge cases and alternative views.</p>
Clarity (0.10)	<p>Focuses on readability, organization, and precision.</p> <p>1–3: Unintelligible or incoherent.</p> <p>4–6: Hard to follow due to verbosity or poor structure.</p> <p>7–8: Understandable but minor awkwardness.</p> <p>9–10: Polished, concise, professional academic tone.</p>
Scoring Protocol	
Penalties	Safety violations, hallucinations, fabricated citations, ignoring constraints, verbosity, or incomplete answers incur -2 to -10 deductions depending on severity.
Bonuses	Exceptional uncertainty handling (+0.5), perfect formatting (+0.3), highly relevant edge cases (+0.5). Bonuses are capped at 10.0.
Final Output	Strictly four numbers: Helpfulness Accuracy Depth Clarity , each with two decimals (e.g., 8.50 9.25 7.00 9.00). No extra text, JSON, or explanation is permitted.

Table 7: Case study examples from WebQA and MultimodalQA, showing how model improves answer grounding compared to text-only and CLIP-VQA baselines.

Examples in WebQA	
Example 1	
Question	“What objects are next to the stanchions on the sidewalk in front of the Spice of Life?”
Ground Truth	Phone booths are next to the stanchions on the sidewalk in front of the Spice of Life.
Text-only	Street signs are next to the stanchions.
CLIP-VQA	Bus stops are next to the stanchions.
HuLiRAG-VQA	Phone booths are next to the stanchions, along with a street sign.
Example 2	
Question	“What hangs in the covered section of Via Amore off Worth Avenue in Palm Beach, Florida?”
Ground Truth	A lantern hangs in the covered section of Via Amore off Worth Avenue in Palm Beach, Florida.
Text-only	There is a hanging shop sign or possibly a banner in the covered walkway, which indicates the presence of a store or restaurant.
CLIP-VQA	A decorative light fixture or chandelier is hanging in the covered section, providing illumination for the walkway.
HuLiRAG-VQA	A lantern is hanging from the ceiling in the covered section, and it appears alongside some decorative elements such as a small sign or plant.
Example 3	
Question	“What tops did the women wear for the discus throw competition at the 2018 Finnish Athletics Championships?”
Ground Truth	Women wore t-shirts and tank tops at the discus throw competition during the 2018 Finnish Athletics Championships.
Text-only	The women were wearing athletic uniforms, such as jerseys and sports bras, which are typical for track and field events.
CLIP-VQA	Most of the women wore sleeveless athletic tops or sports bras, while some had competition singlets.
HuLiRAG-VQA	The women can be seen wearing a mix of t-shirts and sleeveless tops, such as tank tops, with a few athletes also in lighter athletic vests.
Example 4	
Question	“Which organ’s pipes are more golden in color; St Georges Church Organ, Hanover Square, London or Ponce Cathedral pipe organ?”
Ground Truth	St Georges Church Organ is more golden in color compared to the Ponce Cathedral pipe organ.
Text-only	The Ponce Cathedral pipe organ is often described as ornate and golden in appearance, suggesting it is more golden than the one in London.
CLIP-VQA	The pipes of the St Georges Church Organ appear more golden in the image compared to those of the Ponce Cathedral organ.
HuLiRAG-VQA	The St Georges Church Organ pipes look more golden overall, though the Ponce Cathedral organ also has metallic highlights.
Examples in MultimodalQA	
Example 1	
Question	“How many colors are on the Mississippi flag?”
Ground Truth	3 (red, white, blue).
Text-only	The Mississippi state flag traditionally has three main colors, red, white, and blue, though some descriptions also mention gold.
CLIP-VQA	The flag appears to contain red, white, blue, and gold, making it look like four colors in total.
HuLiRAG-VQA	The Mississippi flag shows three clear colors—red, white, and blue—although parts of the emblem may look golden.
Example 2	
Question	“Is Glen E. Friedman’s jacket zipped or unzipped?”
Ground Truth	The jacket is unzipped.
Text-only	It looks like the jacket is usually worn zipped, as most portraits show it closed.
CLIP-VQA	The jacket appears to be zipped, since the front looks mostly closed.
HuLiRAG-VQA	The jacket is unzipped, with the front open and the zipper not fastened, revealing the clothing underneath.
Example 3	
Question	“What is hitting the bongos in the Incredible Bongo Band cover?”
Ground Truth	Hands are hitting the bongos.
Text-only	The bongos are being played with drumsticks or mallets, which are often shown in band artwork.
CLIP-VQA	The bongos are struck by arms, showing a performer energetically playing them.
HuLiRAG-VQA	The bongos are struck by human hands, with both palms clearly shown on the cover.
Example 4	
Question	“What type of ball is the center of the FC Bolosani logo?”
Ground Truth	A soccer ball is at the center of the FC Bolosani logo.
Text-only	The logo likely has basketball in the center, as many European sports clubs are associated with basketball teams, and the round design with simple stripes suggests a basketball rather than a soccer ball.
CLIP-VQA	The middle of the emblem looks like it contains a volleyball-style object, with curved lines across the surface, giving the impression of a volleyball rather than a traditional soccer ball that has hexagonal patches.
HuLiRAG-VQA	At the center of the FC Bolosani crest, there is clearly a soccer ball, with visible hexagonal and pentagonal panels that confirm its design, although some shading and stylization of the logo could make it look slightly different at first glance.